NASA/TM-2000-210328

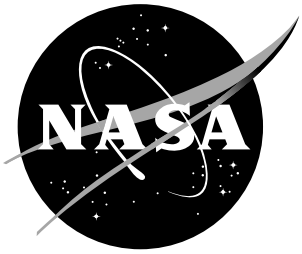

A Comparison of Analytical and Experimental Data for a Magnetic Actuator

Nelson J. Groom
Langley Research Center, Hampton, Virginia

V. Dale Bloodgood, Jr.
Old Dominion University, Norfolk, Virginia

September 2000

The NASA STI Program Office ... in Profile

Since its founding, NASA has been dedicated to the advancement of aeronautics and space science. The NASA Scientific and Technical Information (STI) Program Office plays a key part in helping NASA maintain this important role.

The NASA STI Program Office is operated by Langley Research Center, the lead center for NASA's scientific and technical information. The NASA STI Program Office provides access to the NASA STI Database, the largest collection of aeronautical and space science STI in the world. The Program Office is also NASA's institutional mechanism for disseminating the results of its research and development activities. These results are published by NASA in the NASA STI Report Series, which includes the following report types:

- TECHNICAL PUBLICATION. Reports of completed research or a major significant phase of research that present the results of NASA programs and include extensive data or theoretical analysis. Includes compilations of significant scientific and technical data and information deemed to be of continuing reference value. NASA counterpart of peer-reviewed formal professional papers, but having less stringent limitations on manuscript length and extent of graphic presentations.

- TECHNICAL MEMORANDUM. Scientific and technical findings that are preliminary or of specialized interest, e.g., quick release reports, working papers, and bibliographies that contain minimal annotation. Does not contain extensive analysis.

- CONTRACTOR REPORT. Scientific and technical findings by NASA-sponsored contractors and grantees.

- CONFERENCE PUBLICATION. Collected papers from scientific and technical conferences, symposia, seminars, or other meetings sponsored or co-sponsored by NASA.

- SPECIAL PUBLICATION. Scientific, technical, or historical information from NASA programs, projects, and missions, often concerned with subjects having substantial public interest.

- TECHNICAL TRANSLATION. English-language translations of foreign scientific and technical material pertinent to NASA's mission.

Specialized services that complement the STI Program Office's diverse offerings include creating custom thesauri, building customized databases, organizing and publishing research results ... even providing videos.

For more information about the NASA STI Program Office, see the following:

- Access the NASA STI Program Home Page at ***http://www.sti.nasa.gov***

- E-mail your question via the Internet to help@sti.nasa.gov

- Fax your question to the NASA STI Help Desk at (301) 621-0134

- Phone the NASA STI Help Desk at (301) 621-0390

- Write to:
  NASA STI Help Desk
  NASA Center for AeroSpace Information
  7121 Standard Drive
  Hanover, MD 21076-1320

NASA/TM-2000-210328

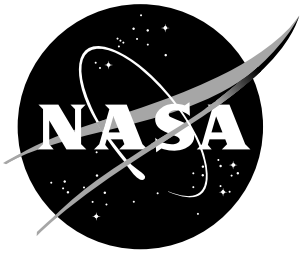

A Comparison of Analytical and Experimental Data for a Magnetic Actuator

Nelson J. Groom
Langley Research Center, Hampton, Virginia

V. Dale Bloodgood, Jr.
Old Dominion University, Norfolk, Virginia

National Aeronautics and
Space Administration

Langley Research Center
Hampton, Virginia 23681-2199

September 2000

Available from:

NASA Center for AeroSpace Information (CASI)
7121 Standard Drive
Hanover, MD 21076-1320
(301) 621-0390

National Technical Information Service (NTIS)
5285 Port Royal Road
Springfield, VA 22161-2171
(703) 605-6000

SUMMARY

Theoretical and experimental force-displacement and force-current data are compared for two configurations of a simple horseshoe, or bipolar, magnetic actuator. One configuration utilizes permanent magnet wafers to provide a bias flux and the other configuration has no source of bias flux. The theoretical data are obtained from two analytical models of each configuration. One is an ideal analytical model which is developed under the following assumptions: (1) zero fringing and leakage flux, (2) zero actuator coil mmf loss, and (3) infinite permeability of the actuator core and suspended element flux return path. The other analytical model, called the extended model, is developed by adding loss and leakage factors to the ideal model. The values of the loss and leakage factors are calculated from experimental data. The experimental data are obtained from a magnetic actuator test fixture, which is described in detail. Results indicate that the ideal models for both configurations do not match the experimental data very well. However, except for the range around zero force, the extended models produce a good match. The best match is produced by the extended model of the configuration with permanent magnet flux bias.

INTRODUCTION

This paper presents theoretical and experimental force-displacement and force-current data for two configurations of a simple horseshoe, or bipolar, magnetic actuator. One configuration utilizes permanent magnet wafers to provide a bias flux and the other configuration has no source of bias flux. The theoretical data are obtained from two analytical models of each configuration. One is an ideal analytical model which is developed under the following assumptions: (1) zero fringing and leakage flux, (2) zero actuator coil mmf loss, and (3) infinite permeability of the actuator core and suspended element flux return path. The ideal models for each configuration are developed using the approach detailed in reference 1. The other analytical model, called the extended model, is developed by adding loss and leakage factors to the ideal model. The values of the loss and leakage factors are calculated from experimental data. The experimental data are obtained from a magnetic actuator test fixture, which is described in detail.

ANALYTICAL MODELS

In this section analytical models of two configurations of a simple horseshoe, or bipolar, magnetic actuator are developed. One configuration, shown schematically in figure 1, has no source of bias flux. The other configuration, shown schematically in figure 2, utilizes permanent magnet wafers mounted on the pole faces to provide a bias flux. The analytical models consist of an ideal model and an extended model. The ideal model is developed using the approach detailed in reference 1 under the following assumptions: (1) zero fringing and leakage flux, (2) zero actuator coil mmf loss, and (3) infinite actuator core and suspended element flux return path permeability. The extended model is developed by adding loss and leakage factors to the ideal model.

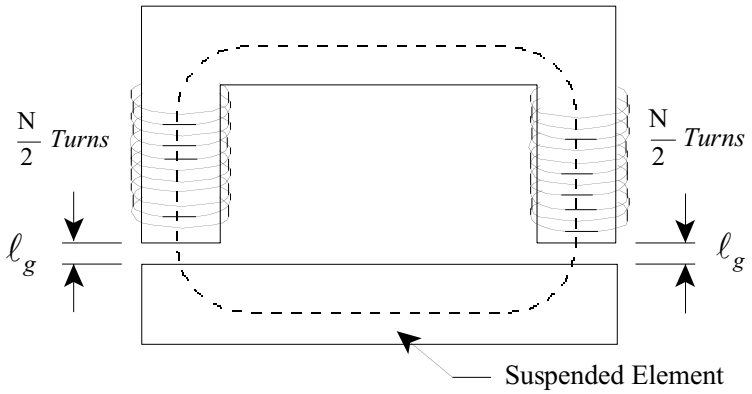

Figure 1.- Magnetic Actuator with No Flux Bias

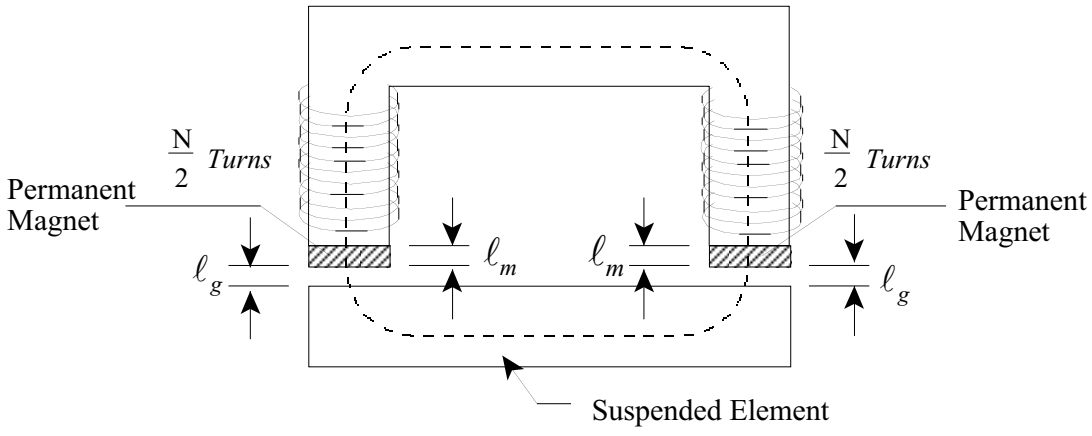

Figure 2.- Magnetic Actuator with Permanent Magnet Flux Bias

Magnetic Actuator With No Flux Bias

Ideal Model.- Taking the line integral around the contour shown in figure 1 results in

$$\oint_C H \bullet d\ell = 2H_g\ell_g + H_a\ell_a + H_s\ell_s \tag{1}$$

where H_g is the magnetic field intensity in the air gap, ℓ_g is the length of one air gap, H_a is the magnetic field intensity in the actuator core, ℓ_a is the length of the contour in the actuator core, H_s is the magnetic field intensity in the suspended element, and ℓ_s is the length of the contour in the suspended element. Magnetic actuators are designed to operate about a nominal specified gap, which will be defined as g_0. If up is defined as positive in figure 1, the air gap length, ℓ_g, can be written in terms of g_0 as

$$\ell_g = g_0 - x \tag{2}$$

where x is the displacement of the suspended element with respect to g_0. Using the relationship

$$\oint_C H \bullet d\ell = \int_S J \bullet n da \tag{3}$$

results in

$$2H_g\ell_g + H_a\ell_a + H_s\ell_s = Ni \tag{4}$$

Using the constitutive relationship

$$B = \mu H \tag{5}$$

where μ is the permeability of the media being considered, equation (4) can be written as

$$2B_g\ell_g + \mu_0\left(\left(\frac{B_a}{\mu_a}\right)\ell_a + \left(\frac{B_s}{\mu_s}\right)\ell_s\right) = \mu_0 Ni \tag{6}$$

Since μ_a and μ_s are assumed to be infinite and B_a and B_s are finite inside the actuator core and suspended element flux return path, the term $\mu_0\left(\left(\frac{B_a}{\mu_a}\right)\ell_a + \left(\frac{B_s}{\mu_s}\right)\ell_s\right)$ becomes zero. Solving for the magnetic flux density in the actuator gaps results in

$$B_g = \frac{\mu_0 Ni}{2\ell_g} \tag{7}$$

From reference 1 the force produced by the magnetic actuator can be written as

$$F_m = \frac{\mu_0 A_g (Ni)^2}{4\ell_g^2} \tag{8}$$

Using equation (7), the force as a function of flux density becomes

$$F_m = \frac{B_g^2 A_g}{\mu_0} \tag{9}$$

Extended Model.- In a typical magnetic actuator with a ferromagnetic core and suspended element flux return path, the permeability is relatively large but finite. Also, there are actuator coil mmf losses. In order to account for these effects, loss factors can be added to the ideal model. Since the permeability of the core and suspended element flux return path is large, the term $\mu_0\left(\left(\frac{B_a}{\mu_a}\right)\ell_a + \left(\frac{B_s}{\mu_s}\right)\ell_s\right)$ is relatively small and can be combined with the term $2B_g\ell_g$ and accounted for by the introduction of the loss factor K_a. To account for actuator coil mmf losses, the loss factor K_i is introduced. Adding K_a and K_i into equation (6) results in

$$2K_a B_g \ell_g = \mu_0 K_i Ni \tag{10}$$

The flux in the gaps becomes

$$B_g = \frac{\mu_0 K_i Ni}{2K_a \ell_g} \tag{11}$$

Equation (11) can be further simplified by defining the combined loss factor, K_L, as

$$K_L = \frac{K_i}{K_a} \tag{12}$$

Equation (11) then becomes

$$B_g = \frac{\mu_0 K_L Ni}{2\ell_g} \tag{13}$$

and the actuator force, from equation (9), becomes

$$F_m = \frac{\mu_0 A_g (K_L Ni)^2}{4\ell_g^2} \tag{14}$$

Magnetic Actuator With Permanent Magnet Flux Bias

Ideal Model.- Using equation (3) and taking the line integral around the contour shown in figure 2 results in

$$2H_g\ell_g + 2H_m\ell_m = Ni \tag{15}$$

In order to determine the permanent magnet operating point, i is set to zero and equation (15) becomes

$$\frac{H_g}{H_m} = -\frac{\ell_m}{\ell_g} \tag{16}$$

Also, the flux in the air gaps is equal to the flux through the permanent magnet wafers

$$B_g A_g = B_m A_m \tag{17}$$

which can be written as

$$\frac{B_g}{B_m} = \frac{A_m}{A_g} \tag{18}$$

Combining (16) and (18) results in

$$\frac{\ell_m}{\ell_g}\left(\frac{A_m}{A_g}\right) = \frac{V_m}{V_g} = -\frac{B_g H_g}{B_m H_m} \tag{19}$$

where V_m and V_g is the volume of the permanent magnet and air gap respectively. A good approximate model for a permanent magnet made of hard magnetic material, such as Samarium Cobalt or Neodymium Iron Boron, is shown in figure (3).

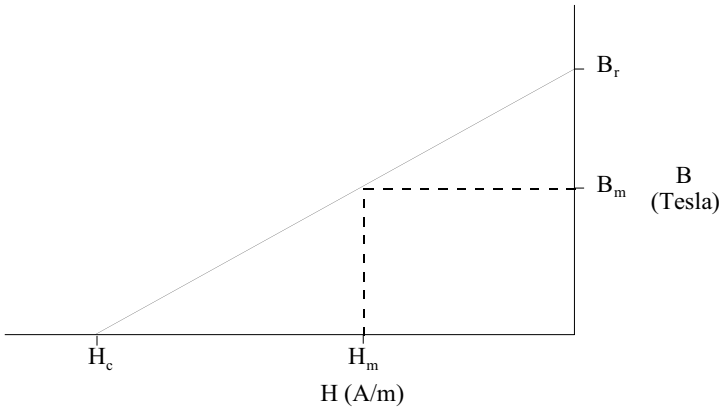

Figure 3.- Ideal B-H Curve For Neodymium Iron Boron

The flux in the magnet can be written as

$$B_m = \mu_m H_m + B_r \tag{20}$$

where $\mu_m = \frac{B_r}{H_c}$, B_r is the residual induction, and H_c is the coercive force. The normal approach in a permanent magnet flux bias design is to minimize the volume of permanent magnet material. From equation (19) it can be seen that in order to minimize V_m, the energy product, $B_m H_m$, must be maximized. Substituting from equation (20), the energy product, $B_m H_m$, becomes

$$B_m H_m = \frac{B_r H_m^2}{H_c} + B_r H_m \tag{21}$$

The energy product is max when $\frac{d(B_m H_m)}{dH_m} = 0$

$$\frac{d(B_m H_m)}{dH_m} = 2\left(\frac{B_r}{H_c}\right) H_m + B_r = 0 \tag{22}$$

From equation (22)

$$H_m = -\frac{H_c}{2} \tag{23}$$

and B_m becomes (from eq. (20))

$$B_m = \frac{B_r}{2} \tag{24}$$

From equations (5) and (16)

$$B_g = -\mu_0 H_m \frac{\ell_m}{\ell_g} \tag{25}$$

Substituting from equation (20) and rearranging terms results in

$$B_g = \frac{\mu_0}{\mu_m}\left(B_r - B_m\right)\frac{\ell_m}{\ell_g} \tag{26}$$

From equation (17)

$$B_g = B_m \frac{A_m}{A_g} \tag{27}$$

In most permanent magnet flux bias actuator designs (including the actuator used in the test fixture described in this paper)

$$A_m = A_g = A_a \tag{28}$$

Also, for permanent magnet material

$$\frac{\mu_0}{\mu_m} \approx 1 \tag{29}$$

Substituting equations (27), (28), and (29) into equation (26) results in

$$B_m = \left(B_r - B_m\right)\frac{\ell_m}{\ell_g} \tag{30}$$

Substituting equation (24) into equation (30) results in

$$\ell_m = \ell_g \tag{31}$$

At the specified operating point, from equation (2), ℓ_m becomes

$$\ell_m = g_0 \tag{32}$$

From equations (5) and (20), equation (15) can be written as

$$2B_g + 2\left(\frac{\mu_0}{\mu_m}\right)\left(B_m - B_r\right)\ell_m = \mu_0 Ni \tag{33}$$

Rearranging terms and substituting from equation (17) results in

$$B_g = \frac{\mu_0\left(Ni + 2\left(\frac{\mu_0}{\mu_m}\right)\frac{B_r\ell_m}{\mu_0}\right)}{2\left(\ell_g + \left(\frac{\mu_0}{\mu_m}\right)\left(\frac{A_g}{A_m}\right)\ell_m\right)} \tag{34}$$

Equation (34) can be further simplified by substituting equations (28) and (29)

$$B_g = \frac{\mu_0\left(Ni + \frac{2B_r\ell_m}{\mu_0}\right)}{2\left(\ell_g + \ell_m\right)} \tag{35}$$

The actuator force, from equation (9), becomes

$$F_m = \frac{\mu_o A_g\left(Ni + \frac{2B_r\ell_m}{\mu_0}\right)^2}{4\left(\ell_g + \ell_m\right)^2} \tag{36}$$

Extended Model.- Adding the loss factors K_a and K_i into equation (15) results in

$$2K_a H_g\ell_g + 2H_m\ell_m = K_i Ni \tag{37}$$

In addition to mmf losses, there is also flux leakage. To account for flux leakage, the leakage factor, K_F, is added to equation (17) which results in

$$K_F B_g A_g = B_m A_m \tag{38}$$

Following through the previous development, equation (33) becomes

$$2K_a B_g\ell_g + 2\left(\frac{\mu_0}{\mu_m}\right)\left(B_m - B_r\right)\ell_m = \mu_0 K_i Ni \tag{39}$$

and from equation (38), equation (35) becomes

$$B_g = \frac{\mu_0\left(K_i Ni + \dfrac{2B_r\ell_m}{\mu_0}\right)}{2\left(K_a\ell_g + K_F\ell_m\right)} \tag{40}$$

From equation (9) the actuator force becomes

$$F_m = \mu_0 A_g \frac{\left(K_i Ni + \dfrac{2B_r\ell_m}{\mu_0}\right)^2}{4\left(K_a\ell_g + K_F\ell_m\right)^2} \tag{41}$$

DESCRIPTION OF TEST FIXTURE

A simplified schematic of the magnetic actuator test fixture is shown in Fig. 4.

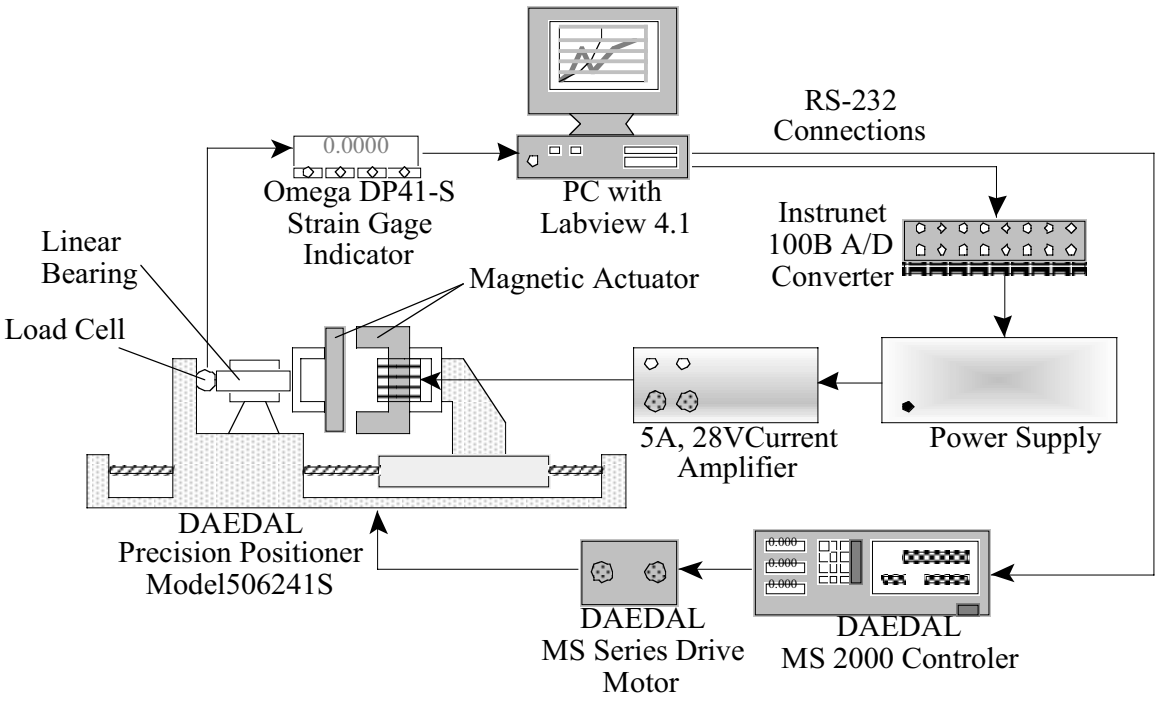

Figure 4.- Schematic Of Magnetic Actuator Test Fixture

The stator was mounted to a precision positioner by an aluminum mounting bracket. The armature was connected to a load cell through an aluminum mounting bracket and aluminum shaft. The shaft was supported by a linear bearing, which restrained the

movement of the armature to 2 degrees-of-freedom, roll about the axial axis of the shaft and lateral movement in the direction of the stator. The shaft was allowed to rotate slightly so that torques would not be transmitted to the load cell, resulting in only the lateral force being measured. The load cell had a maximum range of 50 lb. The positioner was controlled by a PC using Labview 4.1. The signal from the load cell was conditioned by a digital strain gauge indicator and then recorded by Labview. The actual test fixture is shown in Figs. 5 and 6.

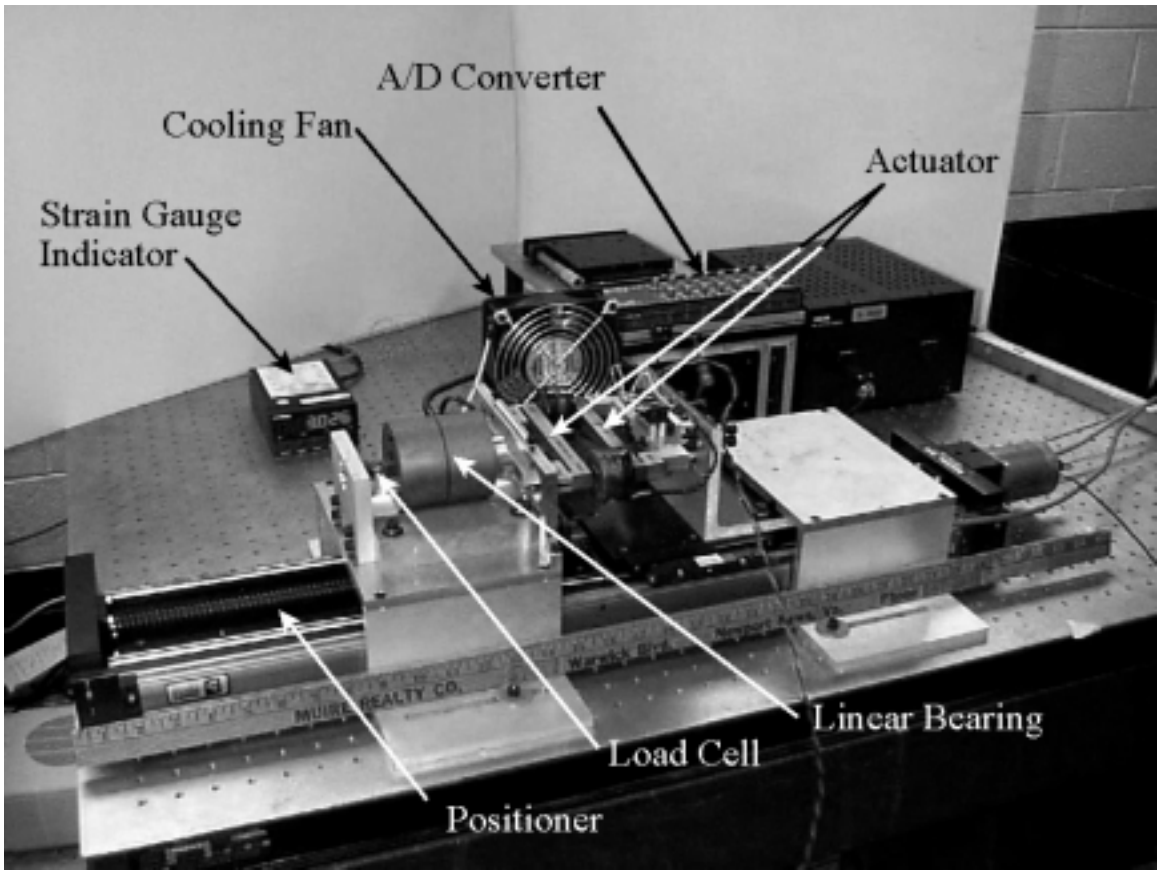

Figure 5.- Magnetic Actuator Test Fixture

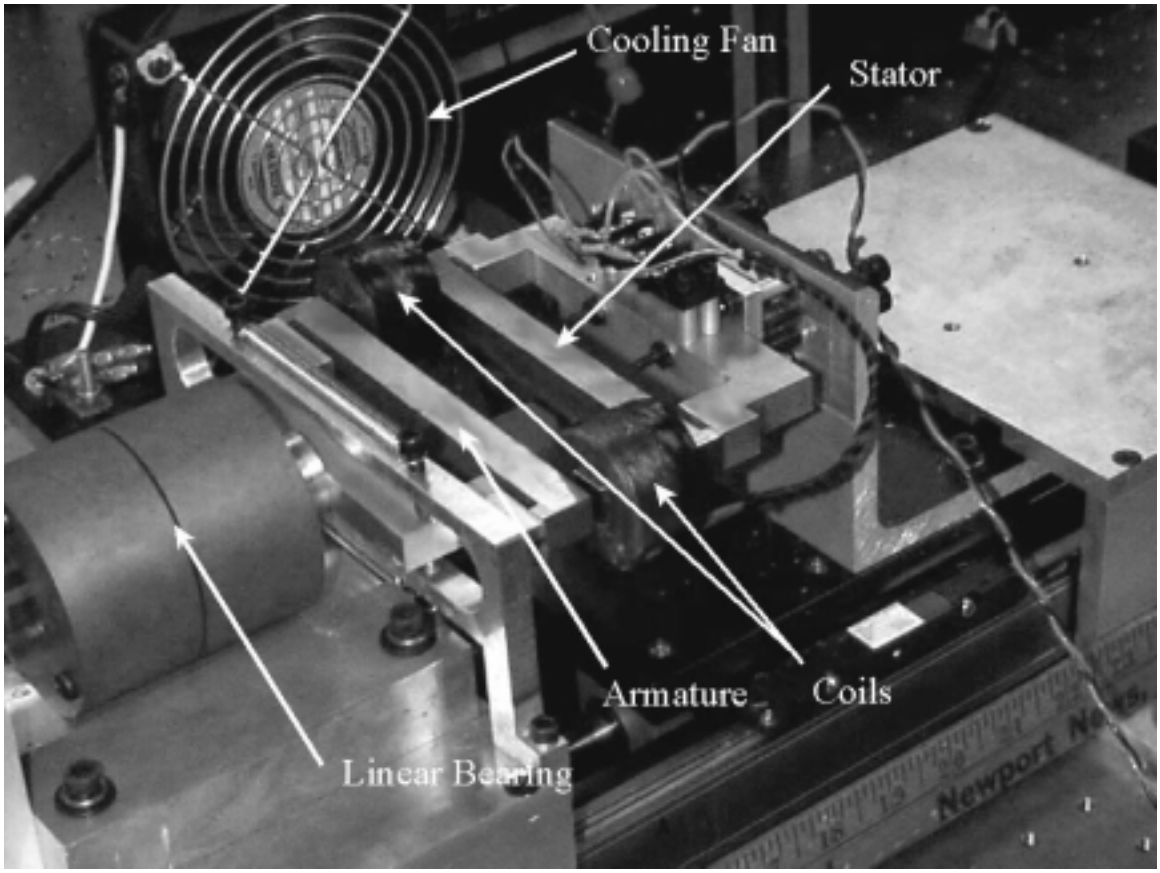

Figure 6.- Magnetic Actuator

The actuator components were constructed from a Connecticut Metal CMI-C cold drawn iron rod. This material is manufactured for use in electromagnetic applications and has a very low carbon content. The B-H curve for the material is shown in Fig. 7. The permanent magnets for the permanent magnet flux bias configuration were constructed of Neodymium-Iron-Boron (Nd-Fe-B) with a residual induction of 1.35 Tesla and a coercivity of -9.7×10^5 A/m. The nominal operating gap for the magnetic actuator was set at 0.05 in. which set the permanent magnet thickness at 0.05 in. also (see eq. 32). The B-H curve for the Nd-Fe-B is shown in Fig. 8.

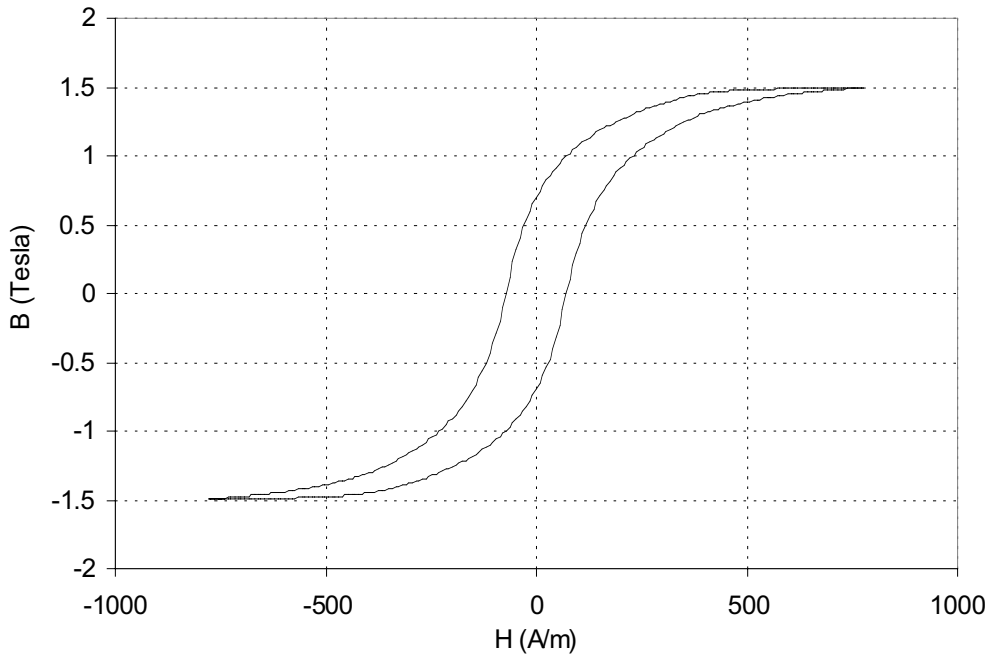

Figure 7.- B-H Curve for Connecticut Steel CMI-C Cold Drawn Steel

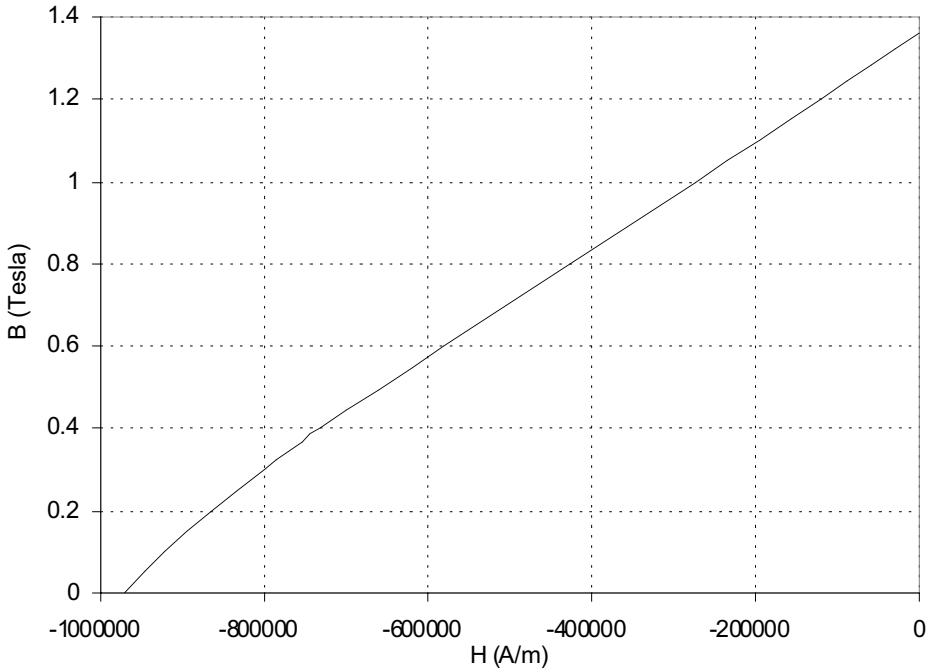

Figure 8.- B-H Curve for Neodymium-Iron-Boron Permanent Magnet

The magnetic actuator design consisted of a simple horseshoe shaped stator and a rectangular armature as shown in Fig. 9.

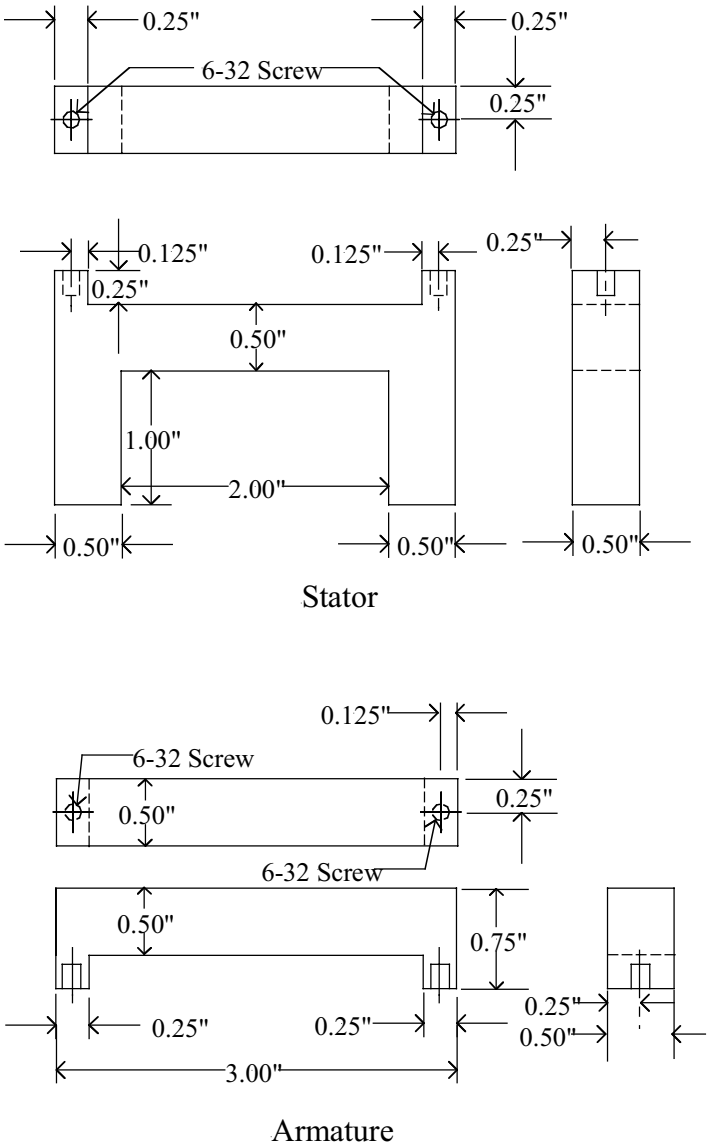

Figure 9.- Design Of Magnetic Actuator Stator and Armature

The stator and the armature had constant cross sectional areas of 0.25 in^2. The stator had a pole separation of 2 inches and a pole length of 1 inch. Both the stator and the armature had extensions located on the back side corners to connect with the aluminum support brackets. These were used to insure that the connection bolts did not reduce the cross sectional area of the magnetic circuit and induce saturation. The connection extensions were located at the edge of the stator and armature to minimize the effect on the magnetic circuit, as is illustrated in Fig. 10.

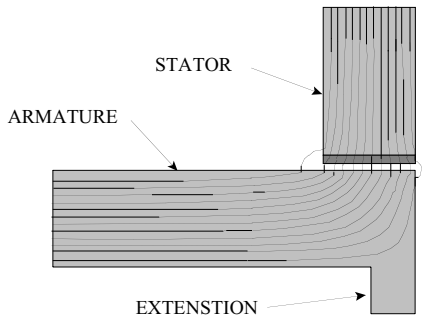

Figure 10.- Magnetic Potential Lines Near Connection Extensions

The magnetic actuator had two coils, one per pole. The coils were connected in series and each coil had 1000 turns. The two coils had resistances of 9.32 Ω and 9.35 Ω.

Each set of measurements was performed five times. The final data presented in Appendix A is the average of the five data sets. The system was calibrated before and after each experiment. The calibration procedure is described in detail in Appendix A. To minimize hysterisis effects, the measurements were recorded in an increasing manner, i.e. the force increment between data points was always positive, except when the force was driven past the zero point of the actuator. The first measurement was taken at the negative limit of the ampere-turns (minimum force) then proceeded to the positive limit (maximum force). For each data point, the system was allowed to settle for 8 seconds to allow the strain gauge signal to settle before the force was recorded.

The zero gap distance was set using the positioner and controller. The two poles of the stator were lined up parallel with the armature. Once the two poles were parallel with the armature, the positioner was advanced in 0.0001Ó increments toward the armature. For the actuator with no flux bias, the positioner was moved until the armature and stator came in contact and the load cell registered a reading. The positioner was then initialized to zero displacement. For the actuator with flux bias, as the positioner moved the stator toward the armature, the attractive force from the permanent magnet increased. At the point of contact between the stator and the armature the force began to decrease. That point was determined within 0.0001Ó and the positioner was initialized to zero displacement.

COMPARISON OF IDEAL MODEL AND TEST FIXTURE RESULTS

As mentioned earlier, the nominal operating gap for the magnetic actuator was set at 0.05 in. Therefore, the results presented in the following sections are for this gap length.

Magnetic Actuator With No Flux Bias

A plot of the ideal model and test fixture results for the magnetic actuator with no flux bias is presented in figure 11. A second order trendline is drawn through the test fixture data points.

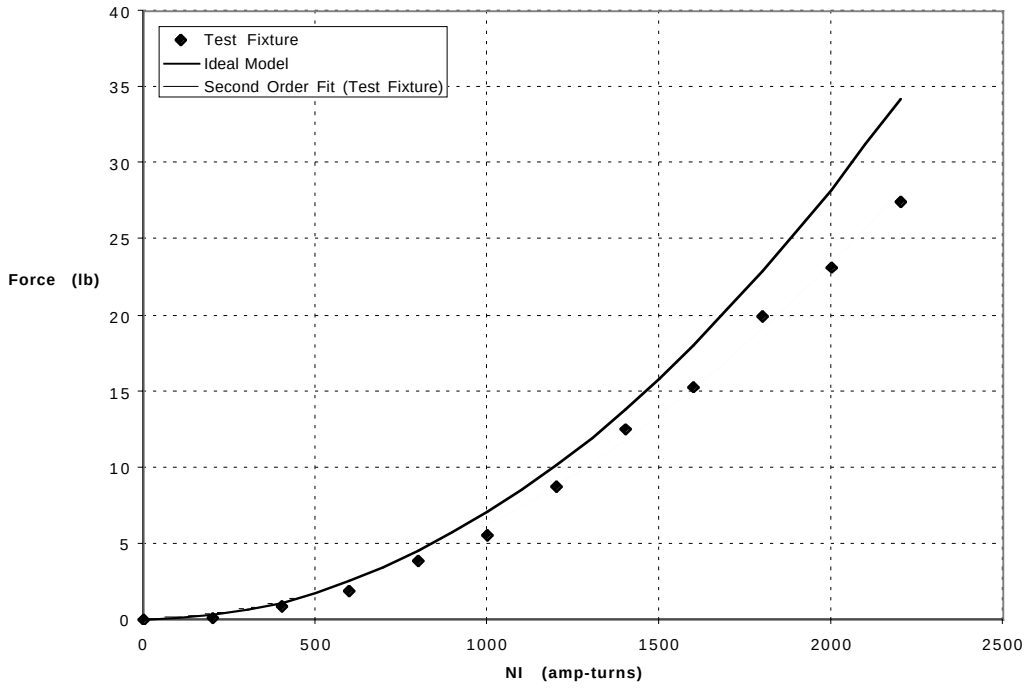

Figure 11.- Ideal Model And Test Fixture Results For Magnetic Actuator with No Flux Bias (ℓ_g = 0.05 in.)

A plot of the percent (%) difference between data points obtained from the test fixture (from the second order trendline) and ideal model is presented in figure 12. The percent difference is defined as

$$\%\ Difference = \left(\frac{F_{fixture} - F_{ideal}}{F_{fixture}} \right) 100 \qquad (42)$$

As can be seen from figure 11, the ideal model results differ significantly from the test fixture results. From figure 12 the percent difference between the test fixture results and the ideal model approaches —22% at Ni = 2200 amp-turns. Since the ideal model predicts a force of 34.2 lb. at Ni = 2200 amp-turns, this translates into a difference of approximately —6.1 lb.

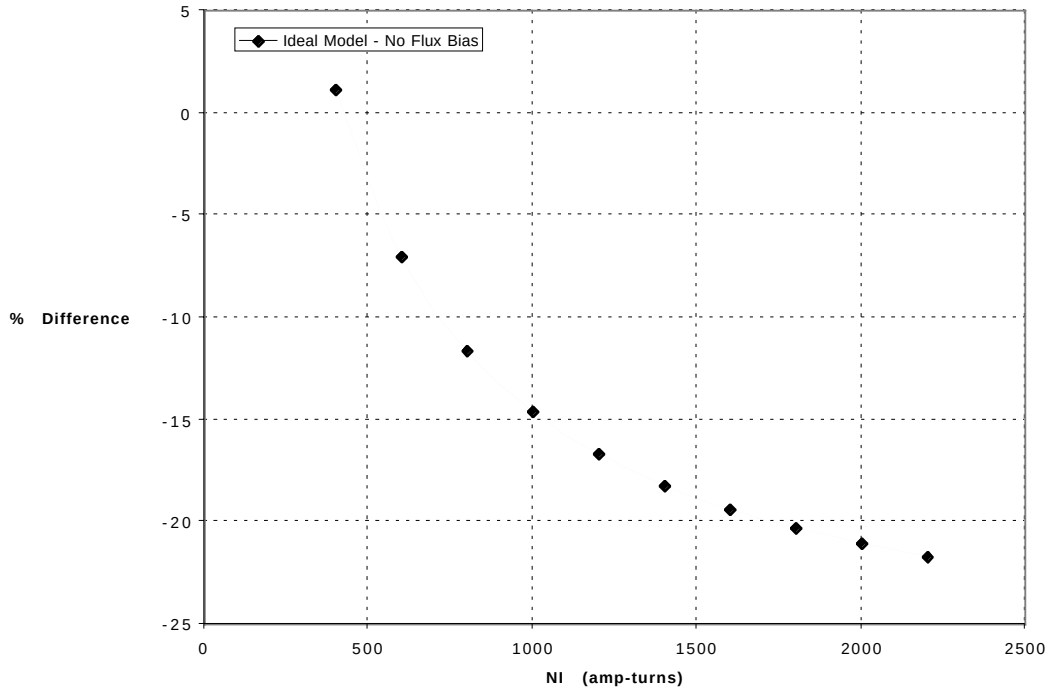

Figure 12.- % Difference Between Test Fixture And Ideal Model Results For Magnetic Actuator With No Flux Bias (ℓ_g = 0.05 in.)

Magnetic Actuator With Permanent Magnet Flux Bias

A plot of the ideal model and test fixture results for the magnetic actuator with permanent magnet flux bias is presented in figure 13. A second order trendline is drawn through the test fixture data points.

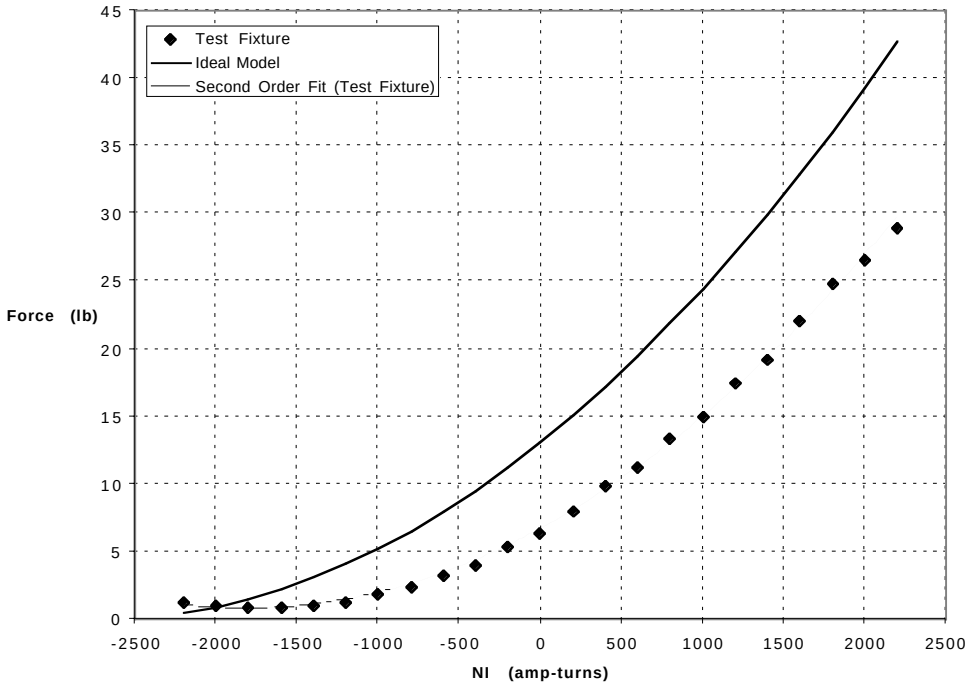

Figure 13.- Ideal Model And Test Fixture Results For Magnetic Actuator with Permanent Magnet Flux Bias (ℓ_g = 0.05 in.)

A plot of the percent difference between data points obtained from the ideal model and test fixture data (from the second order trendline) is presented in figure 14. Figure 13 indicates that the difference between the ideal model results and the test fixture results for the permanent magnet flux bias configuration is greater than that for the configuration with no flux bias. The ideal model predicts that the force will go to zero at approximately Ni = -2728 amp-turns. However, the test fixture results go through a minimum of approximately 0.76 lb. at approximately Ni = -1800 amp-turns and starts to increase as Ni is increased in the negative direction. By modeling the actuator with Vector Fields PC-OPERA 2D, it was determined that as the flux through the permanent magnet wafers is driven near zero, the leakage around the wafers increases significantly and the flux flow undergoes a complex transition. This increase in leakage, together with the complex transition in flux flow, prevents the flux, and hence the force, from being driven to zero. From figure 14 it can be seen that the percent difference between the test fixture results and the ideal model peaks at approximately —194% at Ni = -1400 amp-turns and approaches —44% at Ni = 2200 amp-turns.

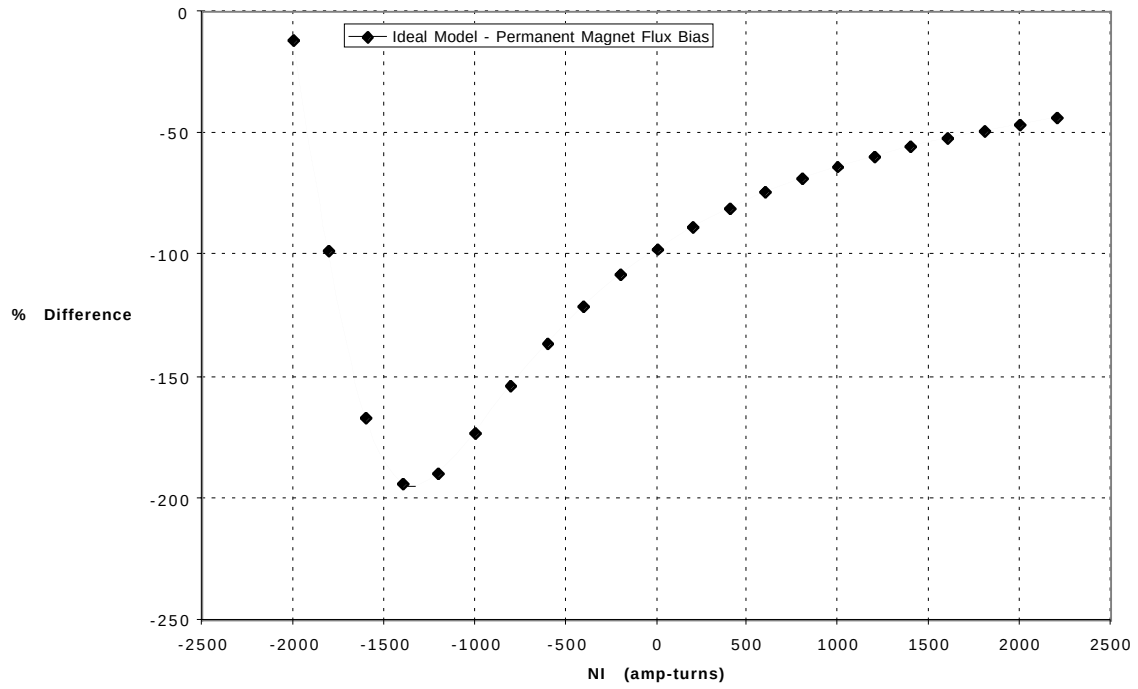

Figure 14.- % Difference Between Test Fixture And Ideal Model Results For Magnetic Actuator With Permanent Magnet Flux Bias (ℓ_g = 0.05 in.)

CALCULATION OF EXTENDED MODEL CONSTANTS

In this section, loss and leakage factors for the extended models developed earlier are calculated using experimental data presented in Appendix A.

Magnetic Actuator With No Flux Bias

The force produced by the extended model of the magnetic actuator with no flux bias is given by equation (14), which can be rewritten as

$$K_L = \left(\frac{2\ell_g}{Ni}\right)\sqrt{\frac{F_m}{\mu_0 A_g}} \tag{43}$$

The combined loss factor, K_L, can be calculated at a given gap and current by substituting values from table A-1 into equation (43). A least squares solution of K_L at a given gap can be obtained by substituting values of Ni and F_m for a range of Ni into equation 43 and using the generalized inverse (ref. 2) to solve the resulting set of equations. Calculating K_L for ℓ_g = 0.05 in. over the range of Ni = 200 — 2200 amp-turns results in K_L = 0.9155.

Magnetic Actuator with Permanent Magnet Flux Bias

The force produced by the extended model of the magnetic actuator with permanent magnet flux bias is given by equation (39), which can be rewritten as

$$\begin{bmatrix} 2\ell_g & 2\ell_m \end{bmatrix} \begin{bmatrix} K_a \\ K_F \end{bmatrix} = \left(\sqrt{\frac{\mu_0 A_g}{F_m}} \right) \left(K_i Ni + \frac{2B_r \ell_m}{\mu_0} \right) \tag{44}$$

The loss and leakage constants can be calculated independently of K_i by setting $i = 0$

$$\begin{bmatrix} 2\ell_g & 2\ell_m \end{bmatrix} \begin{bmatrix} K_a \\ K_F \end{bmatrix} = \left(\sqrt{\frac{\mu_0 A_g}{F_m}} \right) \left(\frac{2B_r \ell_m}{\mu_0} \right) \tag{45}$$

The measured force produced by the magnetic actuator with $i = 0$ is obtained from the $Ni = 0$ row of table A-2. A least squares fit for K_a and K_F over the range of gaps presented in table A-2 can be obtained by substituting the values of force and gap into equation (45) and solving the resulting set of equations using the generalized inverse. Solving for K_a and K_F results in K_a = 1.821 and K_F = 1.005. The loss factor, K_i, can then be calculated at a given gap, over a range of Ni presented in table A-2, by using equation (44). Solving for K_i at ℓ_g = 0.05 in., over the range Ni = 400 — 2200 amp-turns, using the generalized inverse results in K_i = 1.394.

COMPARISON OF EXTENDED MODEL AND TEST FIXTURE RESULTS

This section presents a comparison between extended models, using the loss and leakage factors calculated above, and test fixture results. The results are for a gap length of 0.05 in.

Magnetic Actuator With No Flux Bias

A plot of the extended model and test fixture results for the magnetic actuator with no flux bias is presented in figure 15. A second order trendline is drawn through the test fixture data points.

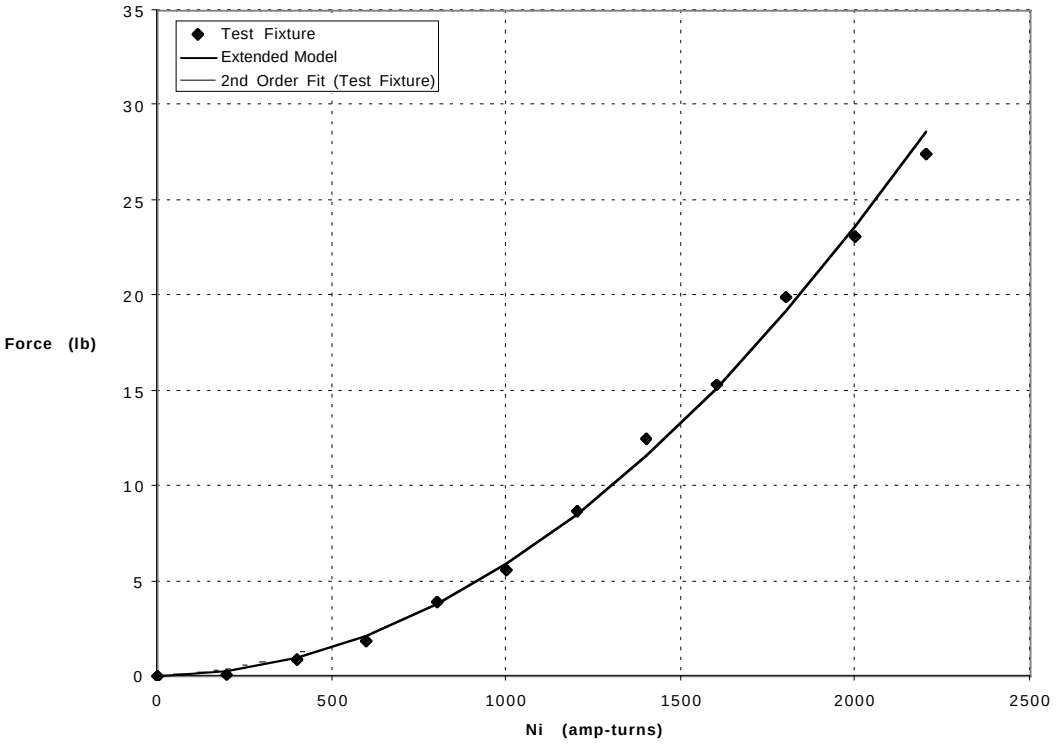

Figure 15.- Extended Model And Test Fixture Results For Magnetic Actuator With No Flux Bias (ℓ_g = 0.05 in.)

A plot of the % difference between data points obtained from the test fixture (from the second order trendline) and the extended model is presented in figure 16. As with the ideal model, the percent difference is defined as

$$\% \, Difference = \left(\frac{F_{fixture} - F_{extended}}{F_{fixture}} \right) 100 \qquad (46)$$

Figure 15 indicates that the extended model data matches the test fixture data much better than the ideal model. From figure 16 the percent difference between the test fixture results and the extended model varies from approximately 10% at Ni = 600 amp-turns to approximately —2% at Ni = 2200 amp-turns. However, the percent difference becomes larger as Ni approaches zero. These results indicate that the extended model would be useful for designing systems that use a single actuator operating against a bias force but not necessarily for a system that uses opposing actuators to produce a bidirectional force with high accuracy requirements around zero force (ref. 3).

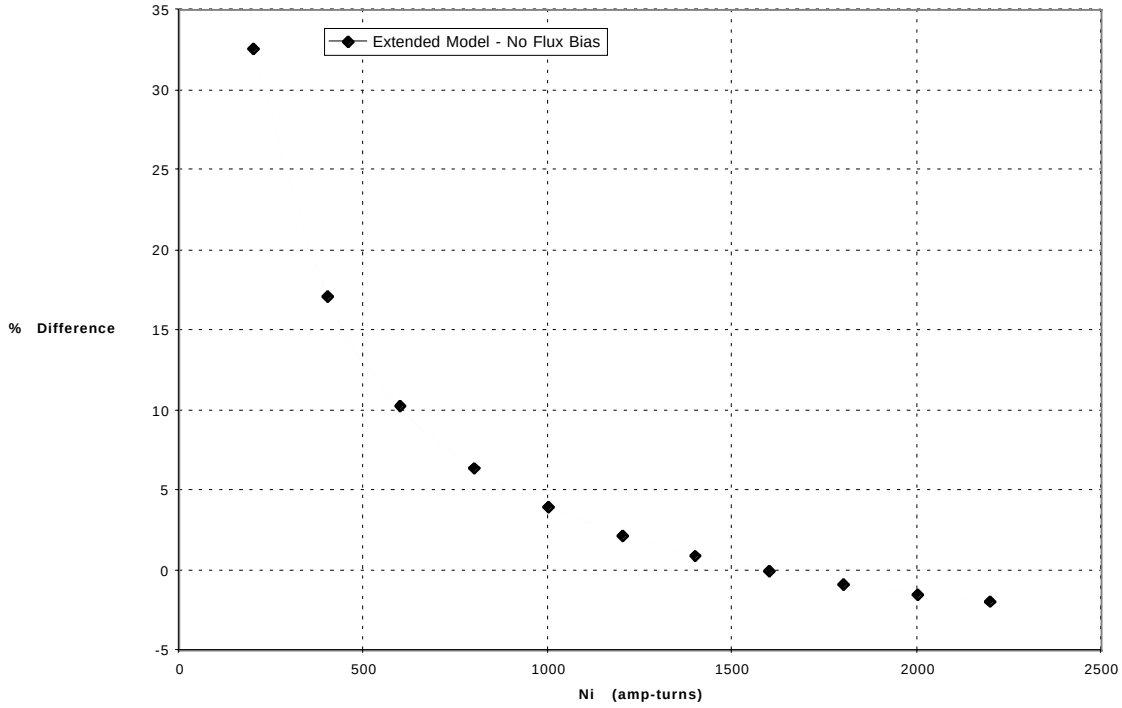

Figure 16.- % Difference Between Test Fixture And Extended Model Results For Magnetic Actuator With No Flux Bias (ℓ_g = 0.05 in.)

Magnetic Actuator With Permanent Magnet Flux Bias

A plot of the extended model and test fixture results for the magnetic actuator with permanent magnet flux bias is presented in figure 17. A second order trendline is drawn through the test fixture data points.

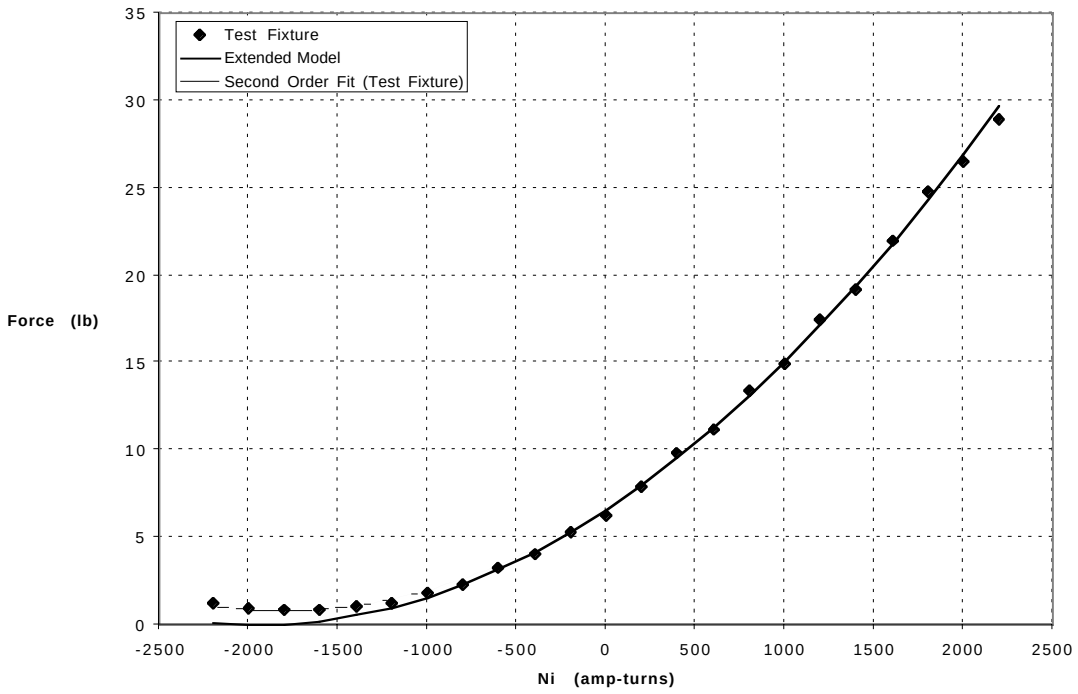

Figure 17 .- Extended Model And Test Fixture Results For Magnetic Actuator With Permanent Magnet Flux Bias (ℓ_g = 0.05 in.)

A plot of the percent difference between data points obtained from the test fixture data (from the second order trendline) and extended model is presented in figure 18. As can be seen from figure 17, the match between the test fixture data and extended model is very good from Ni = -800 amp-turns to Ni = 2200 amp-turns. From figure 18 the percent difference between test fixture and extended model data goes from approximately 11% at Ni = -800 amp-turns to approximately 0% at Ni = 200 amp-turns and remains approximately 0% from Ni = 200 amp-turns to Ni = 2200 amp-turns. The large percent differences between Ni = -800 amp-turns and Ni = -2200 amp-turns is due to the force offset which was discussed previously. These results indicate that the extended model of the magnetic actuator with permanent magnet flux bias would be useful for designing systems that use opposing actuators that are operated differentially about the bias flux provided by the permanent magnets (see ref. 3 for a description of this approach).

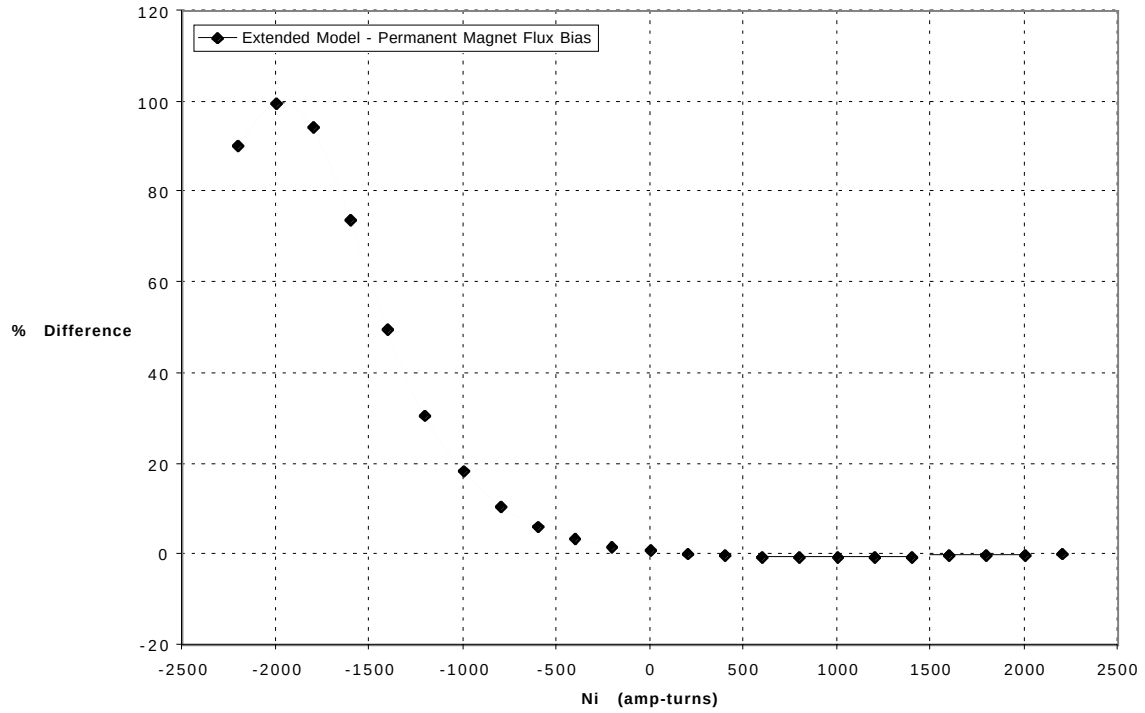

Figure 18.- % Difference Between Test Fixture And Extended Model Results For Magnetic Actuator With Permanent Magnet Flux Bias (ℓ_g = 0.05 in.)

CONCLUDING REMARKS

Magnetic Actuator With No Flux Bias

A comparison of ideal model and test fixture results indicates that the percent difference between the force measured by the magnetic actuator test fixture and the force predicted by the ideal model approaches —22% at Ni = 2200 amp-turns. The extended model, which adds loss and leakage factors to the ideal model, improves the difference to —2% at Ni = 2200 amp-turns. However, the percent difference for the extended model becomes larger than the ideal model as Ni approaches zero. This indicates that the extended model would be useful for designing systems that use a single actuator operating against a bias force but not necessarily for a system that uses opposing actuators to produce a bidirectional force with high accuracy requirements around zero force.

Magnetic Actuator With Permanent Magnet Flux Bias

The difference between ideal model results and test fixture results for the permanent magnet flux bias configuration is greater than that for the configuration with no flux bias. The percent difference between the force measured by the test fixture and the force predicted by the ideal model peaks at approximately —194% at Ni = -1400 amp-turns and approaches —44% at Ni = 2200 amp-turns. The extended model improves the match between measured and predicted values of force significantly over the full range of Ni but in particular over the range from Ni = -800 amp-turns to Ni = 2200 amp-turns. The percent difference goes from approximately 11% at Ni = -800 amp-turns to approximately 0% at Ni = 200 amp-turns and remains approximately 0% from Ni = 200 amp-turns to Ni = 2200 amp-turns. This indicates that the extended model of the magnetic actuator with permanent magnet flux bias would be useful for designing systems that use opposing actuators that are operated differentially about the bias flux provided by the permanent magnets.

APPENDIX

The experimental data used in this report is given in Tables A-1 and A-2. The test fixture was calibrated immediately before and immediately after each test. The average of these two tests was used to calibrate experimental data. The calibration setup is shown in Fig. A-1.

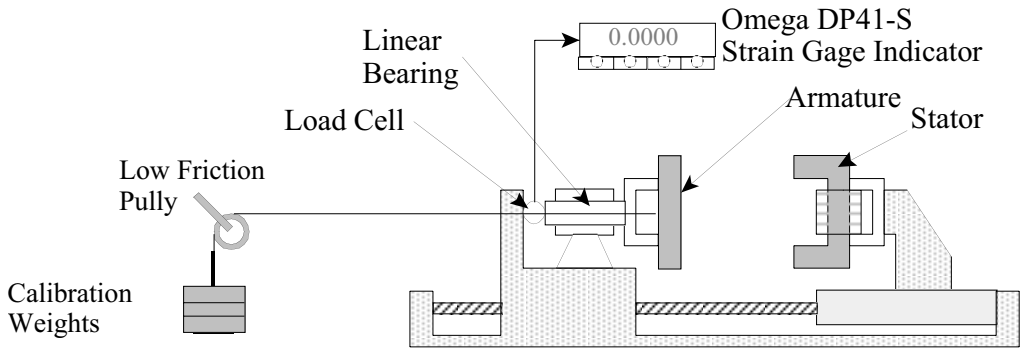

Figure A1.- Calibration Setup For Magnetic Bearing Test Fixture

The load cell was tested at three different weights: 5 lb, 15 lb, and 20 lb. Each weight was measured 5 times with the average recorded and used to calibrate the system.

The range of the five measurements was recorded for each calibration test, for each of the three weights. The ranges were then used to determine the 3σ standard deviation. The maximum 3σ distribution for the three weights indicated a margin of error of 0.18 lb. The ranges for each calibration weight are shown in Figs. A-2, A-3, and A-4.

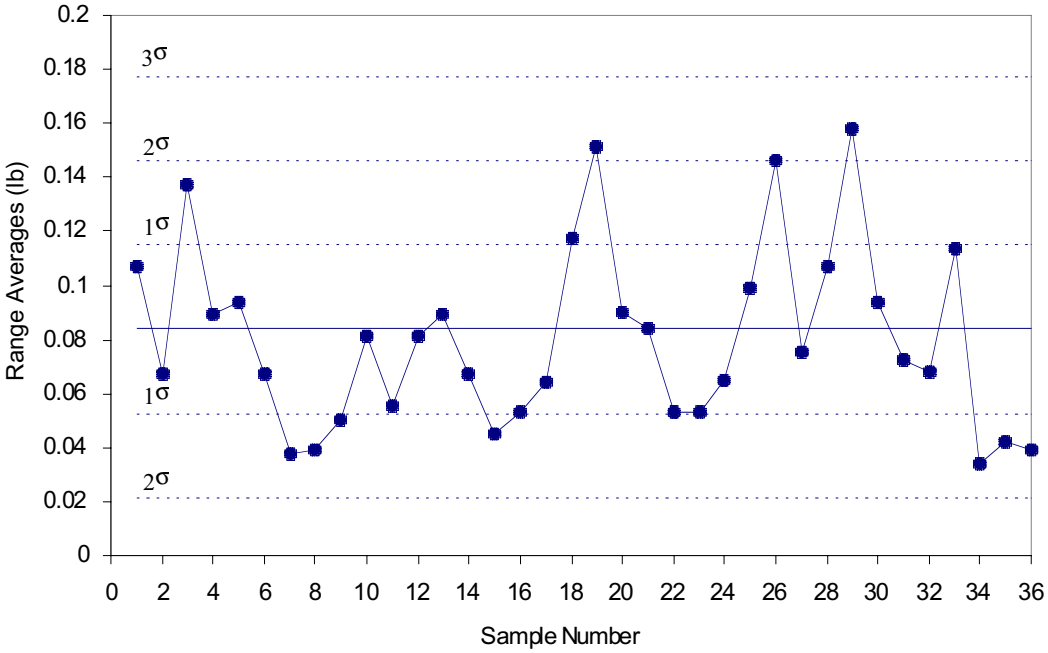

Figure A2.- Standard Deviation of 5 lb. Calibration Data

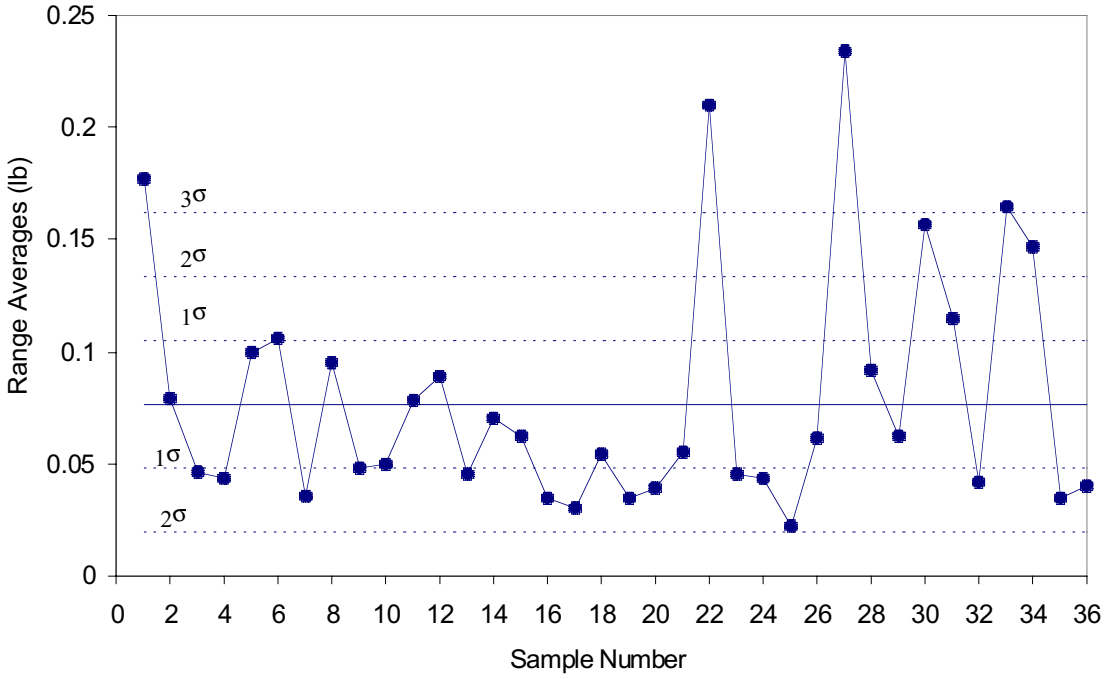

Figure A3.- Standard Deviation of 15 lb. Calibration Data

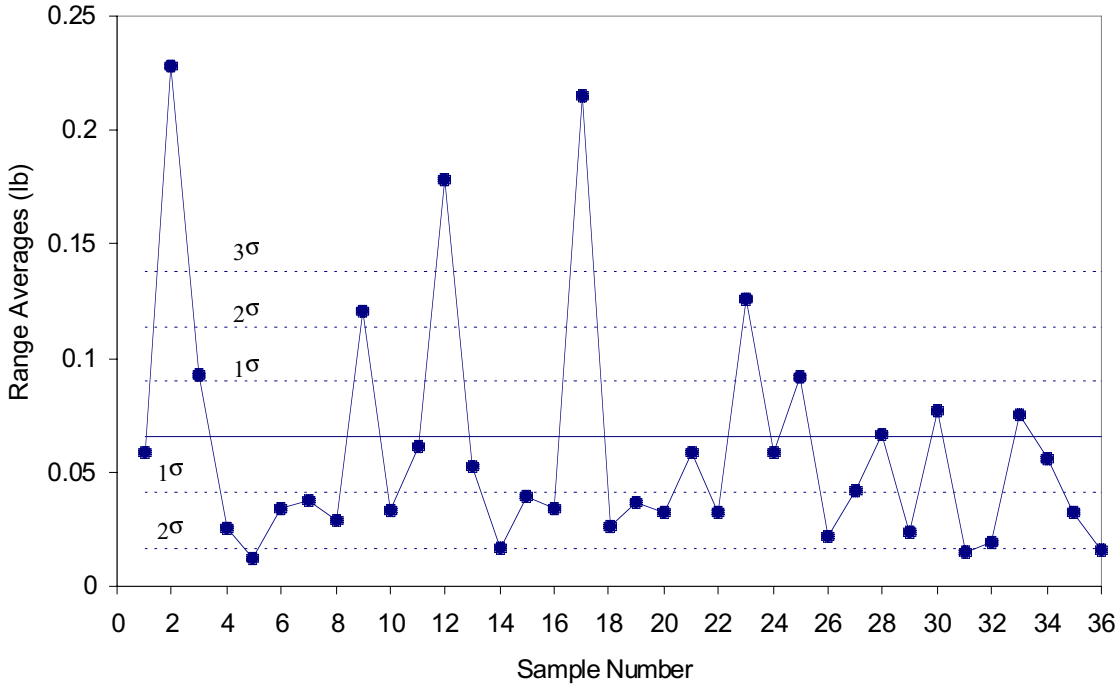

Figure A4.- Standard Deviation of 20 lb. Calibration Data

	Force (lb)				
NI (A)	0.02 in	0.04 in	0.05 in	0.06 in	0.07 in
0	NA*	0.00	0.00	0.00	0.00
200	NA	0.18	0.12	0.05	0.02
400	NA	1.37	0.92	0.61	0.44
600	NA	2.75	1.87	1.31	0.97
800	NA	5.68	3.90	2.79	2.12
1000	NA	8.14	5.59	4.04	3.09
1200	NA	12.70	8.71	6.33	4.86
1400	NA	18.22	12.48	9.08	6.99
1600	NA	22.23	15.29	11.12	8.56
1800	NA	27.73	19.98	14.60	11.25
2000	NA	30.67	23.14	17.03	13.15
2200	NA	34.20	27.43	20.77	16.22

Table A-1: Experimental results for Magnetic Actuator with no Bias Flux

NI	Force (lb)				
(Amps)	0.02 in	0.04 in	0.05 in	0.06 in	0.12 in
-2200	1.905	1.32	1.26	1.10	0.62
-2000	1.637	1.03	0.95	0.81	0.44
-1800	1.661	0.97	0.85	0.71	0.35
-1600	2.055	1.09	0.85	0.68	0.28
-1400	2.563	1.32	1.04	0.80	0.28
-1200	3.726	1.92	1.29	0.99	0.32
-1000	4.769	2.47	1.85	1.43	0.44
-800	6.757	3.55	2.34	1.83	0.58
-600	9.284	4.94	3.26	2.58	0.85
-400	11.26	6.03	4.01	3.18	1.08
-200	14.69	7.94	5.30	4.25	1.50
0	17.26	9.38	6.30	5.06	1.83
200	21.58	11.74	7.95	6.43	2.38
400	24.87	13.47	9.82	7.97	3.02
600	30.36	16.32	11.17	9.09	3.49
800	36.4	19.46	13.38	10.92	4.27
1000	40.45	21.70	14.94	12.21	4.82
1200	46.29	25.36	17.48	14.31	5.72
1400	49.16	27.82	19.22	15.77	6.35
1600	53.1	31.47	22.02	18.10	7.36
1800	NA#	33.70	24.82	20.50	8.44
2000	NA	36.60	26.56	22.06	9.18
2200	NA	39.13	28.95	24.32	10.36

Table A-2: Experimental results for Magnetic Actuator with Permanent Magnet Bias Flux

* The epoxy resin on the coils extended more then 0.02" from the bottom of the coil so these tests could not be recorded.

The load cell was calibrated for a maximum force of 50 lb.

REFERENCES

1. Groom, Nelson J.: Analytical Model of an Annular Momentum Control Device (AMCD) Laboratory Test Model Magnetic Bearing Actuator. NASA TM 80099, August 1979.

2. Penrose, R.: A Generalized Inverse for Matrices. Proc. Cambridge Philos. Soc., vol. 51, 1955, pp. 406-413.

3. Groom, Nelson J.: A Magnetic Bearing Control Approach Using Flux Feedback. NASA TM 100672, March 1989.

REPORT DOCUMENTATION PAGE

Form Approved
OMB No. 0704-0188

1. AGENCY USE ONLY (Leave blank)	2. REPORT DATE	3. REPORT TYPE AND DATES COVERED
	September 2000	Technical Memorandum

4. TITLE AND SUBTITLE
A Comparison of Analytical and Experimental Data for a Magnetic Actuator

5. FUNDING NUMBERS
WU 522-17-51-01

6. AUTHOR(S)
Nelson J. Groom
V. Dale Bloodgood, Jr.

7. PERFORMING ORGANIZATION NAME(S) AND ADDRESS(ES)
NASA Langley Research Center
Hampton, VA 23681-2199

8. PERFORMING ORGANIZATION REPORT NUMBER
L-18033

9. SPONSORING/MONITORING AGENCY NAME(S) AND ADDRESS(ES)
National Aeronautics and Space Administration
Washington, DC 20546-0001

10. SPONSORING/MONITORING AGENCY REPORT NUMBER
NASA/TM-2000-210328

11. SUPPLEMENTARY NOTES
Nelson J. Groom: Langley Research Center, Hampton, VA
V. Dale Bloodgood, Jr.: Old Dominion University, Norfolk, VA

12a. DISTRIBUTION/AVAILABILITY STATEMENT
Unclassified-Unlimited
Subject Category 31 Distribution: Standard
Availability: NASA CASI (301) 621-0390

12b. DISTRIBUTION CODE

13. ABSTRACT (Maximum 200 words)
Theoretical and experimental force-displacement and force-current data are compared for two configurations of a simple horseshoe, or bipolar, magnetic actuator. One configuration utilizes permanent magnet wafers to provide a bias flux and the other configuration has no source of bias flux. The theoretical data are obtained from two analytical models of each configuration. One is an ideal analytical model which is developed under the following assumptions: (1) zero fringing and leakage flux, (2) zero actuator coil mmf loss, and (3) infinite permeability of the actuator core and suspended element flux return path. The other analytical model, called the extended model, is developed by adding loss and leakage factors to the ideal model. The values of the loss and leakage factors are calculated from experimental data. The experimental data are obtained from a magnetic actuator test fixture, which is described in detail. Results indicate that the ideal models for both configurations do not match the experimental data very well. However, except for the range around zero force, the extended models produce a good match. The best match is produced by the extended model of the configuration with permanent magnet flux bias.

14. SUBJECT TERMS
Magnetic Actuator; Magnetic Actuator Test Fixture; Magnetic Actuator Loss and Leakage Factors; Magnetic Actuator Analytical Models

15. NUMBER OF PAGES
34

16. PRICE CODE
A03

17. SECURITY CLASSIFICATION OF REPORT	18. SECURITY CLASSIFICATION OF THIS PAGE	19. SECURITY CLASSIFICATION OF ABSTRACT	20. LIMITATION OF ABSTRACT
Unclassified	Unclassified	Unclassified	UL